Title
Analysis and digital 3D modeling of long-range fourier-domain optical coherence tomography images of the pediatric subglottis

Authors
Su, Erica
Sharma, Giriraj K
Chen, Jason
et al.

Publication Date
2014-03-03

DOI
10.1117/12.2052793

Analysis and Digital 3D Modeling of Long-Range Fourier-Domain Optical Coherence Tomography Images of the Pediatric Subglottis

Erica Su[a], Giriraj K. Sharma[a,d], Jason Chen[a], Tony D. Nguyen[a], Alex Wang[a], Ashley Hamamoto[a], Gurpreet S. Ahuja[b,d], Zhongping Chen[a,c] and Brian J-F. Wong[a,d]

[a]Beckman Laser Institute, Univ. of California Irvine, Irvine, CA, USA
[b]Children's Hospital of Orange County, Orange, CA, USA
[c]Dept. of Biomedical Engineering, Univ. of California Irvine, Irvine, CA, USA
[d]Dept. of Otolaryngology-Head & Neck Surgery, Univ. of California Irvine, Irvine, CA, USA

ABSTRACT

In neonatal and pediatric patients who require long-term endotracheal intubation, the subglottic mucosa is most susceptible to injury from the endotracheal tube. At present, there is no diagnostic modality to identify early signs of subglottic mucosal pathology. Fourier-domain optical coherence tomography (FD-OCT) is a minimally-invasive imaging modality which acquires high-resolution, 3D cross-sectional images of biological tissue. FD-OCT of the neonatal and pediatric airways was conducted to evaluate subglottic microanatomy and histopathologic changes associated with prolonged intubation.

FD-OCT of the larynx, subglottis and proximal trachea was conducted in pediatric and neonatal patients. OCT image sets were analyzed by anatomic categorization (airway level), tissue segmentation and mucosa micrometry in MATLAB. Subsequently, OCT data sets were rendered into digital 3D airway models in Mimics software. We report original methods for subglottic OCT image processing and analysis.

Keywords: Optical coherence tomography, airway, pediatric, neonatal, image analysis, segmentation, 3D modeling

1. INTRODUCTION

In neonatal and pediatric intensive care unit (ICU) settings, the subglottic mucosa is most susceptible to ischemia and ulceration following long-term endotracheal intubation for mechanical ventilation.[1,2] If undiagnosed or untreated, subglottic injury can lead to edema, fibrosis and, ultimately, subglottic stenosis (SGS). This results in significant morbidity to the child and can be a therapeutic challenge to otolaryngologists and critical care specialists.

At present, there is no standardized diagnostic modality to identify early signs of SGS. High-resolution computed tomography (CT) exposes patients to ionizing radiation and lacks adequate spatial resolution to characterize tissue microanatomy.[3] The gold standard for diagnosis of SGS remains direct laryngoscopy and bronchoscopy. However, this procedure involves risks of general anesthesia and further airway instrumentation. Most importantly, endoscopy is limited to a surface view of tissue, precluding evaluation of subepithelial mucosa.

Optical coherence tomography (OCT) is a minimally-invasive imaging modality which couples near infrared light with principles of low coherence interferometry.[4] OCT in the neonatal and pediatric airways has been previously reported.[5,6] However, these studies used time domain OCT (TD-OCT) systems which acquired two dimensional (2D) linear images at low imaging speed. Long-range Fourier-domain OCT (FD-OCT) provides high-speed (25 frames/sec), high-resolution (10 μm axial resolution), three dimensional (3D) cross-sectional images of the airway.[7] We report original methodology for airway FD-OCT image analysis including mucosa segmentation, micrometry and rendering of digital 3D airway models.

Photonic Therapeutics and Diagnostics X, edited by Bernard Choi, et al., Proc. of SPIE
Vol. 8926, 89262J · © 2014 SPIE · CCC code: 1605-7422/14/$18 · doi: 10.1117/12.2052793

2. METHODS

Approval for this study was obtained from the human subjects Institutional Review Boards at University of California Irvine, Children's Hospital of Orange County and St. Joe's Hospital of Orange. For each patient, gestational age (GA) at birth (neonatal patients), current age and weight, medical history, total duration of intubation (neonatal patients) and endotracheal tube (ETT) size were recorded from the medical record.

2.1. OCT system and scanning probe

A long-range FD-OCT system was constructed using previously described interferometry specifications.[7] Near-infrared light from a 1310 nm swept source laser (50 kHz A-line scan rate; 109 nm bandwidth at 10 dB; Axsun Technologies, Billerica, MA) is split by a 90-10 coupler into a sample arm (tissue) and reference arm (mirror), respectively. An acousto-optic modulator (AOM; Brimrose Corp., Sparks, MA) was incorporated into the reference arm to generate a frequency shift of 150 Hz for the OCT signal. The AOM allows for maximization of the swept source coherence length, providing axial imaging range up to 25 mm. OCT signal is back-reflected from tissue depths (up to 2 mm) at varying time delays and recombined with the reference arm to generate a reflectivity profile (A-line). Each 360º cross-sectional image consists of 2000 A-lines. Axial resolution is approximately 10 μm, while lateral resolution (increases with radial distance from fiber tip) is approximately 100 μm at the focal point of the signal.

Flexible, fiber-based OCT probes (70-80 cm length) were constructed with 0.7 mm outer diameter (OD). The fiber was coupled distally with a gradient refractive index (GRIN) lens which focused the laser beam on a 45º gold-coated rod mirror to redirect signal at a 90º angle. A custom-designed metal housing (0.7 mm OD) was soldered to the distal end of the coil to enclose and protect the GRIN lens and mirror. In order to withstand high rotational speed of the fiber, a stainless torque coil (Asahi Intecc, Santa Clara, CA) encased the single-mode optical fiber to translate torque from the rotational motor to the distal probe tip. For neonatal OCT, probes were customized to have an active working distance of 4-5 mm, based on approximations of neonatal airway luminal dimensions. For pediatric airways, probes with a working distance of 5-7 mm were constructed.

A fiber optic rotary joint (Princetel Inc., Pennington, NJ) coupled with a rotational motor (Animatics, Santa Clara, CA) allowed for high-speed rotational scanning. A dual motor linear stage (Zaber Technologies Inc., Vancouver, BC) allowed for simultaneous linear pullback of the probe to acquire spiral images in a retrograde fashion. In neonatal and pediatric airways, consecutive 360º axial frames had 62.5 μm and 250 μm separation respectively.

2.2. *In vivo* FD-OCT of the pediatric subglottis

Intraoperative subglottic FD-OCT was conducted in pediatric patients with no history of prolonged intubation or known central airway pathology. This population was imaged in order to gain experience with trans-ETT, high-speed rotational scanning and understanding of normal airway microanatomy on OCT images.

All patients underwent tonsillectomy and/or adenoidectomy for obstructive airway disease. Patients were placed in a supine position, induced with general anesthesia and endotracheally intubated. The total length of the ventilation circuit from an external circuit connector to the distal tip of the ETT was measured and calculated. The OCT probe, encased in a sterilized, transparent fluorinated ethylenepropylene (FEP) sheath (1.37 mm OD), was inserted through the circuit connector and advanced within the ETT until the lens was 1 cm proximal to the ETT tip in the trachea. Trans-ETT images of the laryngotracheal complex were acquired in a spiral, retrograde fashion as the probe was rotated (25 Hz) and retracted (6.25 mm/sec) through the central airway. Total time for probe pullback was approximately 30-35 seconds.

2.3. *In vivo* FD-OCT of the neonatal subglottis

Bedside FD-OCT imaging was conducted in the neonatal ICU in patients who required endotracheal intubation for mechanical ventilation. No changes to mechanical ventilation settings, analgesic or sedation medications were made. In an identical process to intraoperative pediatric imaging, the probe was placed within a sterilized FEP sheath (1.37 mm OD) and advanced through the ventilation circuit until the lens reached 5 mm proximal to the ETT tip. The probe was rotated (12.5 Hz) and retracted (0.781 mm/sec) through the airway as images were acquired. Total time for probe pullback and image acquisition was approximately 20 seconds.

2.4. Tissue Segmentation and Micrometry

Continuous helical scanning of the airway generates 500-800 360º raw images (BMP file format; 2000 x 2048 pixels) in Cartesian coordinates. Data was first evaluated for signal quality, noise levels, and image distortion. Image stacks with low signal:noise ratio, inadequate optical penetration depth or extensive volumes of missing or distorted tissue data were excluded. Only data sets with easily recognizable tissue contours and identifiable anatomical structures were analyzed. Video 1 depicts an image stack in polar coordinates, cropped between the larynx and proximal trachea. Images are displayed at image acquisition speed (12.5 frames/sec) in the order of acquisition (pullback from trachea to larynx).

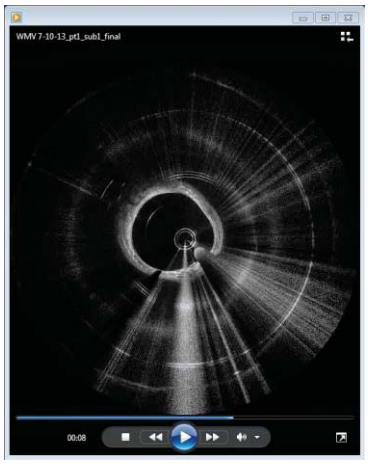

Video 1. OCT images in polar coordinates, from proximal trachea to larynx. http://dx.doi.org/10.1117/12.2052793.1

All segmentation and micrometric analysis was conducted within MATLAB (MathWorks, Natick, MA) programs written by our group. Image stacks were sorted into three anatomic groups: larynx, subglottis, and trachea. This classification was based on user identification of anatomical landmarks within the laryngotracheal complex (cartilage, vocal folds, laryngeal ventricles). Images from other anatomical regions were excluded from the present analysis. Each data subset was imported in linear format (Cartesian coordinates) and analyzed in MATLAB separately. Each 360º frame consists of 2000 individual A-lines. In general, the structures in each image from the top of the image, downwards are: 1) FEP sheath wall, 2) ETT wall, 3) respiratory mucosa epithelium, 4) basement membrane, 5) lamina propria, 6) perichondrium, 7) cartilage. Figure 1 shows representative linear OCT images acquired from the pediatric trachea (Figure 1a) and subglottis (Figure 1b).

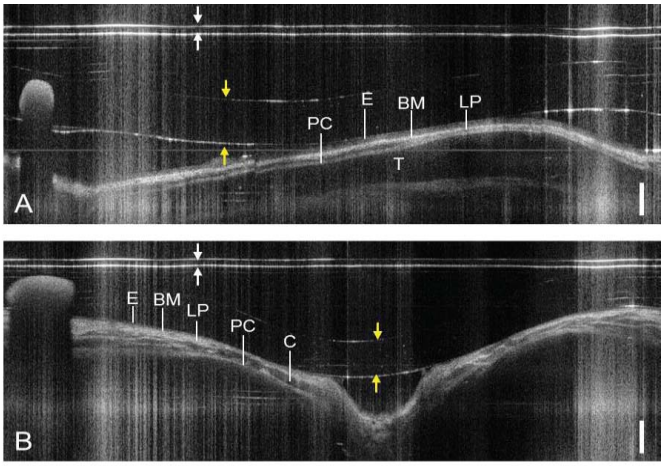

Figure 1. Linear OCT images of pediatric trachea (a) and subglottis (b). White arrows = sheath, yellow arrows = wall of ETT, E = epithelium, BM = basement membrane, LP = lamina propria, PC = perichondrium, T = tracheal cartilage, C = cricoid. Bar = 500 µm.

The use of our software and image processing steps are described below. First, to establish a measurement reference within the image frame, the user was first prompted for the ETT size (2.5 – 3.5 mm inner diameter/ID, recorded from the medical record), which corresponded to a known ETT thickness based on published ID/OD measurements (Portex; Smiths Medical International Ltd., Hythe, Kent, UK). Subsequently, the user identified the inner and outer surfaces of the ETT on the OCT image to calculate the ETT thickness in pixels.

Manual segmentation of the region of interest (respiratory mucosa) was conducted using an Intuos 5 drawing tablet (Wacom; Vancouver, WA) and built-in MATLAB functions (e.g., magnifying tool). Respiratory mucosa tissue is traced, excluding cartilage, ETT and miscellaneous noise/artifact. Artifacts such as stretched segments of data (due to friction between the rotating coil and FEP sheath) or missing data (e.g. absent signal secondary to blood or excessive mucous) were omitted from the tracing. In a single image, tissue segmentation could be accomplished in one large or multiple small tracings (if segments of data consisted of missing/distorted A-lines). Figure 2 depicts the manual segmentation process.

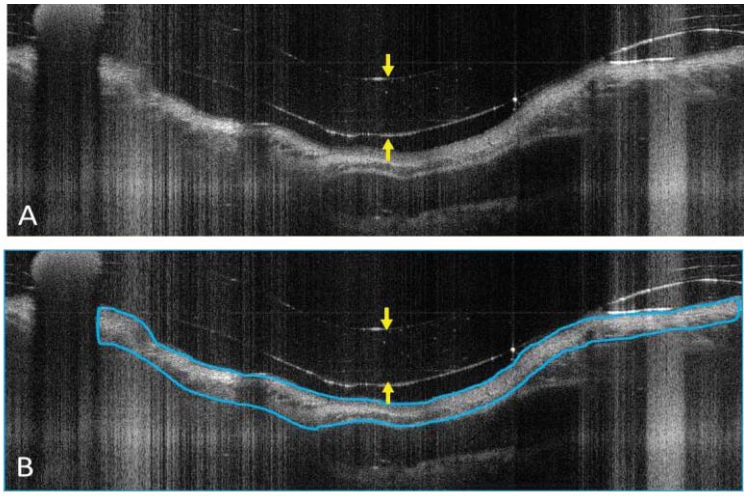

Figure 2. Linear OCT image before (a) and after (b) segmentation. Yellow arrows = ETT wall, blue line = respiratory mucosa outline.

After segmentation of all images within a data subset, the program automatically scans each A-line to measure (in pixels) the vertical distance of the segmented region which is used to calculate tissue thickness. The vertical distances are converted into microns using the equation:

$$T_{\mu m} = (T_{pixel} \times ETT_{\mu m} \times 1.5) / (ETT_{pixel} \times 1.3) \quad (1)$$

where $T_{\mu m}$ is the tissue thickness in micrometers, T_{pixel} is the measured tissue thickness in pixels, $ETT_{\mu m}$ is the ETT thickness in micrometers (reference), and ETT_{pixel} is the measured ETT thickness in pixels. This equation takes the refractive indices of air in plastic (1.5) and tissue (1.3) into account.

The mean, standard deviation and range of mucosal thickness (μm) are calculated for each selected image. Following segmentation of all images in a given stack, averages for all measurement statistics are calculated. Quantitative data is output to a text file within the image directory.

2.5. Rendering of 3D airway model in Mimics

Raw image stacks were processed in MATLAB and image processing software for anatomical scaling, image alignment, antero-posterior orientation and tissue segmentation. Subsequently, image stacks were rendered into 3D airway models. Pre-processing was conducted in the following sequence:

1) Prior to data acquisition, the OCT reference arm length is manually adjusted to focus the airway tissue within the upper one-third of the image frame. This adjustment of interferometry optics is not standardized, and results in

variability (between data sets) of the vertical pixel count between the top of the frame and sample (tissue). In order to render the 3D volumetric data with accurate airway cross-sectional dimensions, this distance must be corrected.

The ID of the FEP sheath was approximately 1.067 mm, and FD-OCT image resolution in air is approximately 8.8 μm/pixel. Hence, the average distance between the probe and the sheath inner surface is approximately 0.533 mm (sheath radius) or roughly 60.5 pixels. Within a graphic viewer (IrfanView; Irfan Skiljan, Austria), the vertical pixel count between the top of the image frame and the FEP sheath was measured and averaged for the image stack. The stack was exported to a MATLAB application where pixel depth is added or subtracted to the top of all images as necessary to attain a 60.5 vertical pixel count.

2) Images were converted from Cartesian to polar coordinates (MATLAB), which provides an anatomical (axial cross-section) orientation to the data.

3) During high-speed rotational scanning, torque is transferred from the proximal motor to the probe tip as the flexible probe (80 cm) bends through the ventilation circuit and airway. Rotation of the fiber assembly along this complex, curved pathway results in the distal tip of the probe to wobble within the lumen of the sheath, leading to shifting of the image center line between consecutive OCT frames. Alignment of successive images is required to form a spatially aligned, 3D data set. Within Amira (FEI Visualization Sciences Group, Burlington, MA), two consecutive images are superimposed in a semi-transparent format to display tissue contours. In the event of misalignment, two different tissue contours are visible, allowing the user to axially shift either image until tissue overlap is achieved. Alignment is performed, in sequence, for each image in the stack.

4) Within IrfanView, image size was decreased from 4096 x 4096 pixels to 512 x 512 pixels to reduce computational time.

5) Post-processed axial images were imported into Mimics (Materialise, Leuven, Belgium) for 3D rendering. The stack was aligned as a whole into correct antero-posterior orientation, with anterior towards the top of the image in standard axial anatomical orientation.

In Mimics, mucosa segmentation was conducted to exclude all intraluminal (sheath, ETT, noise) and extraluminal (cartilage, noise) data from images. Airway tissue was manually segmented slice-by-slice (Intuos 5 drawing tablet) using a wide circular brush to draw over the region of interest and create a mask (Figure 3). Brush pixel size (diameter) was adjustable within and between slices, and was always maintained slightly wider than mucosal thickness.

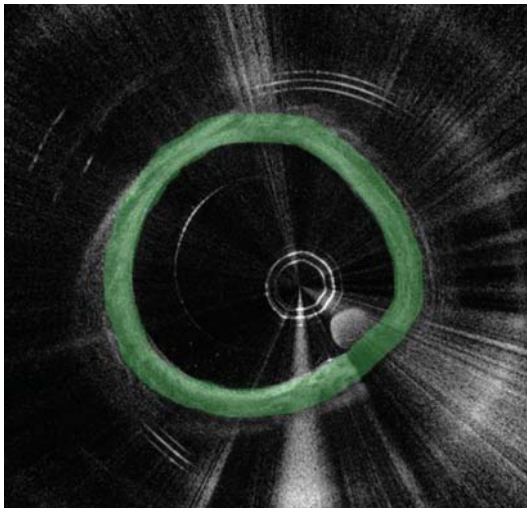

Figure 3. Tissue segmentation in Mimics. Respiratory mucosa outlined with wide brush to create a tissue mask (transparent green outline).

After all images in the stack were manually segmented, tissue masks are rendered into a raw 3D object. Tissue edges were processed using built-in Mimics features including smoothing (4 iterations, 0.9 smoothing factor) and triangle reduction with advanced edge mode (tolerance of 0.05 mm, edge angle of 15 degrees, and 10 iterations). A "wrap" feature in Mimics closed any gaps of volumetric data due to separation between adjacent slices or loss of signal (smallest detail of 0.2 mm, gap closing distance of 1 mm). After wrapping, the 3D model is smoothed one final time (5th iteration, 0.9 smoothing factor). The final 3D airway model of the pediatric laryngotracheal complex is a hollow structure with wall thickness representative of respiratory mucosa (Figure 4).

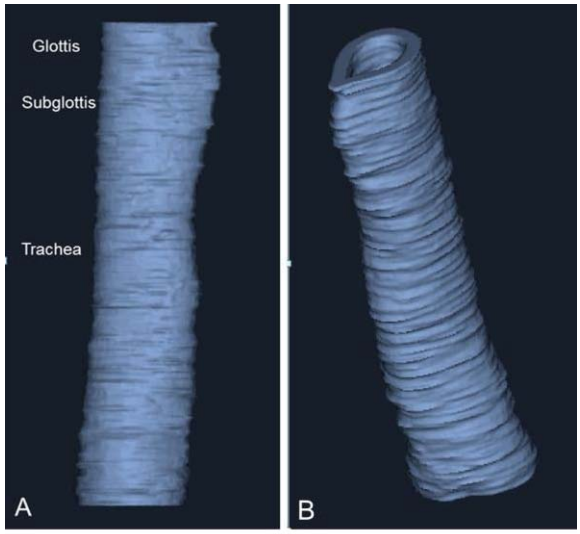

Figure 4. Digital 3D airway model in sagittal (a) and oblique (b) views.

Within Mimics, 3D models may be viewed as static images or in 360º rotation around a user-defined axis. Cross-sectional views of the airway model can be obtained using a "clipping" feature Clipping consists of user-controlled scrolling through 3D cross-sectional views of the airway in axial, sagittal or coronal planes. As the 3D model is clipped in the specified plane, OCT data is visibly overlaid on airway wall. This allows for visualization of the layered microstructure of respiratory mucosa along the entire length of the airway model. Using the "capture movie" feature, videos (AVI file format) of cross-sectional scrolling in a particular plane can be created. This allows the user to pause the video at a cross-section of interest and visualize mucosal microanatomy at adjacent airway levels at once (Figure 5).

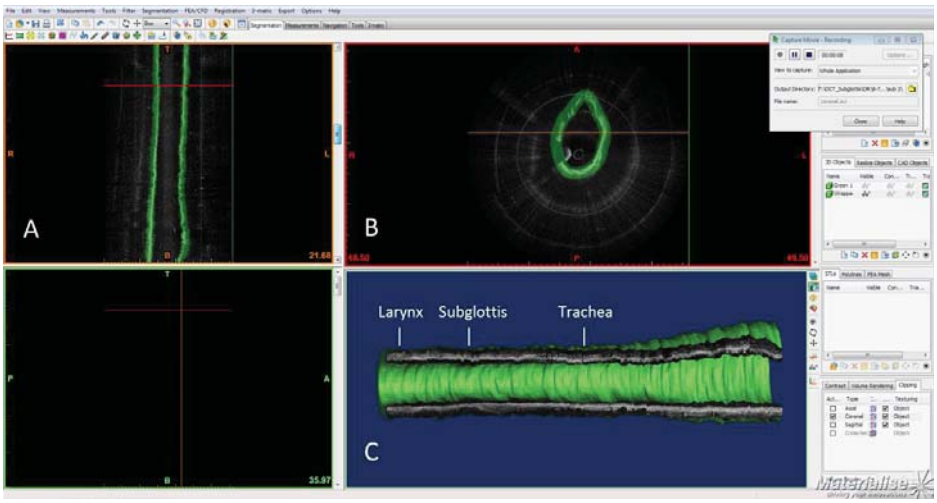

Figure 5. Mimics screenshot of coronal plane of 3D airway model depicting the level of slice in coronal (a) and axial (b) orientations. 3D OCT data overlaid onto airway wall in coronal plane (c).

3. DISCUSSION AND CONCLUSION

At present, there is no standardized means for *in vivo* diagnosis and quantification of subglottic mucosal disease following prolonged endotracheal intubation. FD-OCT-based micrometry of the subglottic mucosa gives clinicians a means to evaluate and serially monitor the degree of mucosal thickening due to glandular dilatation, edema or increased collagen deposition within the lamina propria. We used FD-OCT to image the pediatric subglottis and described semi-automated image analysis methods for tissue segmentation, mucosal micrometry and visualization of 3D volumetric data to assess the extent of mucosal pathology.

While several steps in our methodology are automated, we believe airway OCT image analysis requires a degree of expert user input. Cropping the raw image stack (500-800 images) to airway levels of interest is based upon identification of anatomical landmarks. Further trisecting the cropped image stack into anatomical regions (larynx, subglottis, trachea) requires expertise in recognition of distinct topographical characteristics of the pediatric airway (luminal contours) and anatomical structures (e.g., C-shaped tracheal cartilage, cricoid, thyroid cartilage, vocal folds). Tissue segmentation for micrometry requires precise exclusion of perichondrium, cartilage, artifact and noise from the region of interest to obtain accurate micron-scale measurements. Hence, manual segmentation requires knowledge of pediatric airway microanatomy. Algorithms for tissue surface recognition in OCT images are currently under development in our group. These functions may significantly improve efficiency of image analysis through automated detection of ETT inner and outer surfaces (measurement reference) and mucosal surfaces (segmentation, micrometry, and mask for 3D rendering).

A limitation of our study is the variability in image quality between data sets. OCT probe fabrication is not a standardized process, and results in variable signal strength and signal:noise ratio, as well as segments of blocked signal within individual frames. We account for missing or distorted data by allowing the user to segment partial or multiple regions of interest within an individual frame. In 3D modeling steps, the Mimics "wrap" feature fills in any volumetric gaps of data to provide a smooth airway surface.

In addition to automated tissue surface recognition, future steps include algorithms for mucosal texture analysis based on grey-scale properties of tissue to quantify tissue turbidity (i.e., water and collagen content) and assess the stage of subepithelial disease. Also, tissue segmentation methods based on "fuzzy" connectedness methods pioneered by the Medical Image Processing Group (University of Pennsylvania, Philadelphia, PA) account for uncertainty in tissue edges by representing tissue edges as a "fuzzy" grey-scale gradient as opposed to the binary segmentation methods reported here.[8,9]

The methods described here offer means for OCT-based evaluation of subglottic disease through tissue micrometry and 3D qualitative evaluation of subepithelial histopathology. Serial FD-OCT and micrometry of the pediatric airway mucosa may allow otolaryngologists and critical care specialists to diagnose and monitor the progression of subglottic disease, ultimately aiding in clinical decision making.

REFERENCES

[1] Holinger, P. H., Kutnick, S. L., Schild, J. A., and Holinger, L. D., "Subglottic stenosis in infants and children," Ann Otol Rhinol Laryngol, 85(5 Pt.1), 591-9 (1976).

[2] Walner, D. L., Loewen, M. S., and Kimura, R. E., "Neonatal subglottic stenosis--incidence and trends," Laryngoscope, 111(1), 48-51 (2001).

[3] Dame Carroll, J. R., Chandra, A., Jones, A. S., Berend, N., Magnussen, J. S., and King, G. G., "Airway dimensions measured from micro-computed tomography and high-resolution computed tomography," Eur Respir J, 28(4), 712-20 (2006).

[4] Huang, D., Swanson, E. A., Lin, C. P., Schuman, J. S., Stinson, W. G., Chang, W., Hee, M. R., Flotte, T., Gregory, K., Puliafito, C. A., and et al., "Optical coherence tomography," Science, 254(5035), 1178-81 (1991).

[5] Ridgway, J. M., Ahuja, G., Guo, S., Su, J., Mahmood, U., Chen, Z., and Wong, B., "Imaging of the pediatric airway using optical coherence tomography," Laryngoscope, 117(12), 2206-12 (2007).

[6] Ridgway, J. M., Su, J., Wright, R., Guo, S., Kim, D. C., Barretto, R., Ahuja, G., Sepehr, A., Perez, J., Sills, J. H., Chen, Z., and Wong, B. J., "Optical coherence tomography of the newborn airway," Ann Otol Rhinol Laryngol, 117(5), 327-34 (2008).
[7] Jing, J., Zhang, J., Loy, A. C., Wong, B. J., and Chen, Z., "High-speed upper-airway imaging using full-range optical coherence tomography," J Biomed Opt, 17(11), 110507 (2012).
[8] Grevera, G., Udupa, J., Odhner, D., Zhuge, Y., Souza, A., Iwanaga, T., and Mishra, S., "CAVASS: A computer-assisted visualization and analysis software system," Journal of Digital Imaging, 20, 101-118 (2007).
[9] Udupa, J. K., Odhner, D., Samarasekera, S., Goncalves, R. J., Iyer, K., Venugopal, K., and Furuie, S., "3dviewnix - an Open, Transportable, Multidimensional, Multimodality, Multiparametric Imaging Software System," Image Capture, Formatting, and Display, 2164, 58-73 (1994).